STRUCTURE REPAIR BY ADDITIVE FRICTION STIR DEPOSITION: MECHANICAL RESPONSE OF THE REPAIRED INTERFACE

Florian Girault, Louise Toualbi, Bouilly Thibaut

▶ **To cite this version:**

Florian Girault, Louise Toualbi, Bouilly Thibaut. STRUCTURE REPAIR BY ADDITIVE FRICTION STIR DEPOSITION: MECHANICAL RESPONSE OF THE REPAIRED INTERFACE. ECSSMET 2024, Sep 2024, Noordwijk, Netherlands. hal-04942162

HAL Id: hal-04942162
https://hal.science/hal-04942162v1

Submitted on 12 Feb 2025

HAL is a multi-disciplinary open access archive for the deposit and dissemination of scientific research documents, whether they are published or not. The documents may come from teaching and research institutions in France or abroad, or from public or private research centers.

L'archive ouverte pluridisciplinaire **HAL**, est destinée au dépôt et à la diffusion de documents scientifiques de niveau recherche, publiés ou non, émanant des établissements d'enseignement et de recherche français ou étrangers, des laboratoires publics ou privés.

STRUCTURE REPAIR BY ADDITIVE FRICTION STIR DEPOSITION: MECHANICAL RESPONSE OF THE REPAIRED INTERFACE

Florian Girault [1,2], Louise Toualbi[1], Thibaut Bouilly[3]
[1] *ONERA- the French Aerospace Lab, 29 Av. de la Division Leclerc, 92320 Châtillon, France,*
Email : florian.girault@onera.fr, louise.toualbi@onera.fr
[2] *LMS-CNRS, École polytechnique, 91120 Palaiseau, France*
[3] *CNES, 52 Rue Jacques Hillairet, 75012 Paris, France,*
Email : thibaut.bouilly@onera.fr

ABSTRACT

Two solid-state processes, cold spray and Additive Friction Stir Deposition, are compared with the aim of repairing damaged aerospace structures of reusable satellite launchers. The samples obtained by cold spray feature a material health prohibitive for repair. Conversely, samples repaired by AFSD show excellent microstructural continuity between the substrate and the deposited material. The impact of the process on the microstructure of the repaired part thus obtained is analyzed through fine characterization using scanning electron microscopy. The mechanical response of the repaired structure is analyzed using hardness mapping, as well as tensile tests carried out on specimens sampled at different heights in the deposited material. These results indicate a strong thermo-mechanical impact of the process, both on the substrate and on the deposited material. A revalidation methodology based on the analysis of local deformation gradients by Digital Image Correlation is also described in this paper.

1. INTRODUCTION

Repair or restoration of damaged parts is becoming an industrial issue to reduce costs and increase the lifetime of critical components. In the context of the aerospace industry, additive manufacturing repair is a new field of study that requires the highest attention to safety, i.e. material health. Special care must be taken to ensure the reliability of the repaired parts. To that end, it is necessary to understand the microstructural changes that occur during the repair process and to ensure the associated mechanical properties exhibit no significant discrepancy from those of the initial material.

Among the existing additive manufacturing technologies, several processes are potential candidates for repair. Liquid-state material deposition technologies, such as Direct Energy Deposition, power bed fusion processes, or Wire Laser Additive Manufacturing, provide a strong bond between repaired and initial materials. However, these technologies also induce thermal stresses in both the remanufactured part and the interfacial region, necessitating further heat treatment. In the case of a massive part, this step can present a significant challenge.

Moreover, most of the parts to be repaired are manufactured from structurally hardened aluminum alloys; repairing such components by liquid-phase processes is inherently challenging due to the risk of deleterious effects such as cracking, chemical alteration, or microstructural changes [2,3]. It is important to note that such effects may render the repaired part unsuitable for its intended use. From this perspective, solid-state material deposition technologies, such as cold spray [1] or Additive Friction Stir Deposition (AFSD) [7], appear to be promising for repair.

In a joint effort between CNES and ONERA, the effectiveness of various solid-state processes for the repair of structurally hardened 2000 and 7000 series aluminum alloys has been assessed.

The first phase is to ensure that the repair process allows good material health for the repaired part. The feasibility of these repairs was first validated through a detailed analysis of the material health of the parts obtained, with precise characterization at the interface between the substrate and the deposited material.

Secondly, microstructural alterations associated with the repair process were assessed by means of fine characterization under scanning electron microscopy. The mechanical response of the repaired structure was evaluated by hardness characterization and, on the most promising samples, by a tensile characterization test.

Ultimately, it is crucial to revalidate these repaired structures with respect to their mechanical performance. Therefore, a methodology for analyzing the impact of microstructural heterogeneities on mechanical response is proposed.

This paper focuses on obtaining the first viable repaired samples and the methodology for revalidating the repaired structures.

2. COLD SPRAY

Although initially developed for coating applications, cold spray can be used to deposit thick coatings (of the order of several millimeters), making it highly suitable for repair applications [1]. However, its use is limited to materials with a certain degree of ductility, although the use of helium as a propellant gas and the increased gas

temperature extend the range of eligible materials.

With regard to the alloys of interest for repair, this process offers a decisive advantage for 2000 and 7000 series aluminum alloys: it eliminates the risk of evaporation of the alloy's constituent elements, notably Li and Zn [1,4,5]. This paper presents the results obtained on two structurally hardened aluminum alloys, the industrial grades AA2219 and AA7075, which are widely used in the aerospace industry.

The cold spray technique consists in accelerating a gas through a nozzle. This gas drives the raw material (powder) through the nozzle, leading to a high-speed projection towards the substrate. As the temperature of the propellant gas rises, so does its velocity, accelerating the powder particles until a dense coating adheres to the substrate. However, the gas temperature remains below the melting temperature of the powder, thus avoiding transition to the liquid phase, limiting residual stresses, chemical element evaporation and preserving a fine-grained microstructure. Metallurgical bonding is achieved by the plastic deformation of each powder particle on impact with the substrate. In this paper, all the repaired samples are built using nitrogen gas at a pressure of 4.5 MPa.

Sample geometry

For each of the material/process combinations, a decision was made to produce two simple geometries of the repaired sample, as illustrated in Fig. 1. In consequence, the configuration in question may be defined as a "single-cord" geometry, comprising a monotrack of deposited material with a thickness in the z-direction equivalent to a single pass, or approximately one millimeter. In contrast, the "build-up" geometry consists of two juxtaposed beads with a thickness in the z-direction corresponding to five successive passes of material deposition (approximately 5 mm). These build-up samples are both multitrack and multilayer samples.

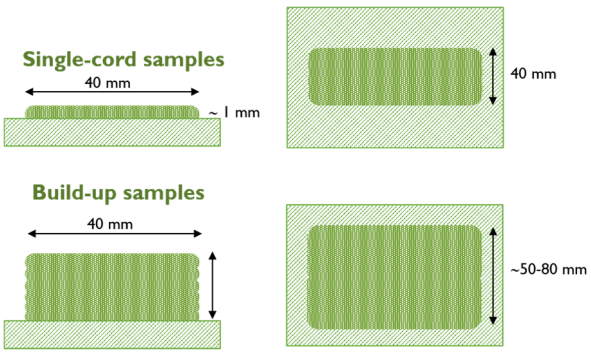

Figure 1: Schematic representation of monolayer and build-up geometries.

The varying parameters are the gas temperature, the scan speed and the stepover amount (for multitracks only). The powder feeding rate is maintained constant at 3 RPM. Each layer is less than 1mm thick, between 200 and 300µm depending on the building parameters: consequently, the so-called “single-cord” samples are in reality composed of 2 to 3 layers of deposited material. To be as representative as possible of a repair situation, the substrates are processed from the same material as the deposited one (homogeneous repair), i.e. AA2219 and AA7075 in temper conditions.

Material health

Fig. 2 shows a cross-section of an AA2219 single-cord sample observed with an optical microscope. The level of porosity observed is extremely high and seems prohibitive for our repair problem. Pores of several micrometers in size are observed along the entire height of the deposit, from the interface to the core of the deposited material.

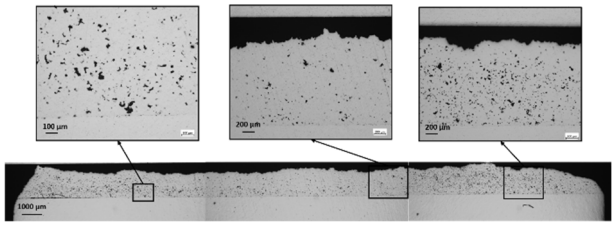

Figure 2: Optical picture of a cross-sectioned AA2219 cold spray single-cord sample.

These initial observations also show areas where the old powder grains (which constitute the filler material) projected onto the substrate are still clearly visible (Fig. 3): this reflects plastic deformation that is too weak to ensure a good adhesion of the repaired area to the damaged part.

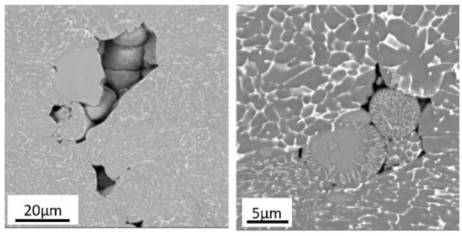

Figure 3: SEM images of AA2219 cold spray single-cord sample - presence of powder grains from the filler material.

Similarly, the first characterizations of AA7075 single-cord sample show an extremely high porosity level, which is prohibitive for our repair problem. In addition, these AA7075 repaired samples feature a pronounced delamination at the interface between the substrate and the deposited material that can extend over several centimeters, depending on the building parameters (Fig. 4).

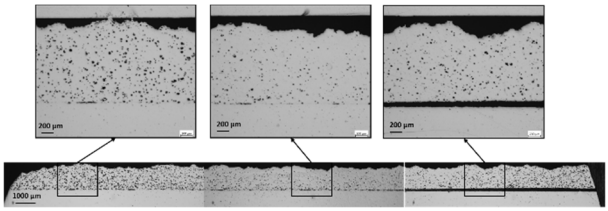

Figure 4: Optical picture of a cross-sectioned AA7075 cold spray monolayer sample.

For both materials studied, the porosity rate and delamination frequency increased with the height of the wall, as illustrated Fig. 5. Thus, the results in terms of material health are even less favorable on the build-up type samples.

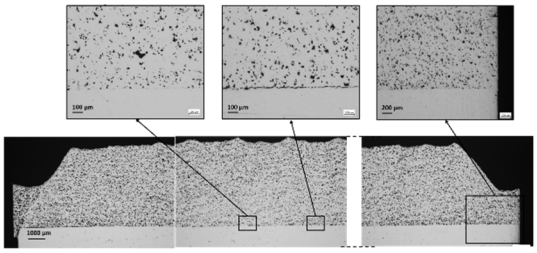

Figure 5 : Optical picture of a cross-sectioned AA2219 cold spray build-up sample.

Microstructural characterization

Electron microscopy characterization provides a better view of the microstructure at the interface. Delamination was detected in all repaired samples. Depending on the manufacturing parameters, this delamination can vary in length from a few hundred micrometers (Fig. 6.a and 6.c) to several centimeters (becoming visible on optical images, as in Fig. 4). Lack-of-fusion-like defects are also present both at the interface and in the core of the deposited material (Fig. 6.b and 6.d).

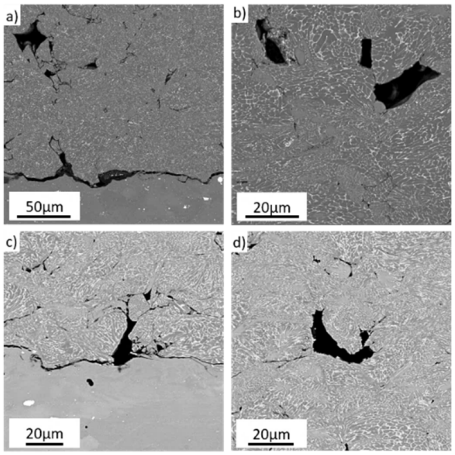

Figure 6 : SEM images of a) AA2219 cold spray single-cord sample – delamination at the interface, b) AA2219 cold spray single-cord sample – lack of fusion, c) AA7075 cold spray single-cord sample – delamination at the interface and d) AA7075 cold spray single-cord sample – lack of fusion.

Regarding microstructural modification, SEM images highlight chemical heterogeneities in the deposited material, which could correspond to the trace of solidification cells, indicating a very high local rise in powder temperature, probably above the melting point. Given the poor material quality of these samples, no further microstructural investigations were carried out to confirm this conjecture.

Mechanical response

Fig. 7 displays a hardness map performed on AA2219 cold spray single-cord sample. The main observations are:

- An abrupt transition between substrate and deposited material, confirming observations of poor adhesion between substrate and deposited material.
- A much lower level of hardness in the deposited zone, as its hardness dropped from 175Hv to 140Hv, which supports the hypothesis of a very high local temperature rise having, if not caused a local melting of the material, at least induced a re-solution of all the hardening precipitates present in the material prior to deposition.

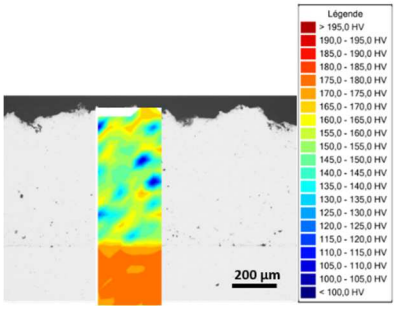

Figure 7 : HV0.2 Vickers hardness map of AA2219 cold spray single-cord sample. Indents are separated by 300µm.

Overall, the cold spray repair results were disappointing and did not meet the needs of our problem. No further work was conducted on the cold spray samples.

3. ADDITIVE FRICTION STIR DEPOSITION

Just like cold spray, AFSD relies on solid-state plastic deformation. Fig. 8 shows the principle of this method: the filler material is put in contact with a substrate and set in rotation. The heat generated by the friction forces softens the material, which then plastically flows. An additional hard shoulder is also used in order to increase heat and deformation. A complete structure can be built by successive passes deposing new layers on top of each other.

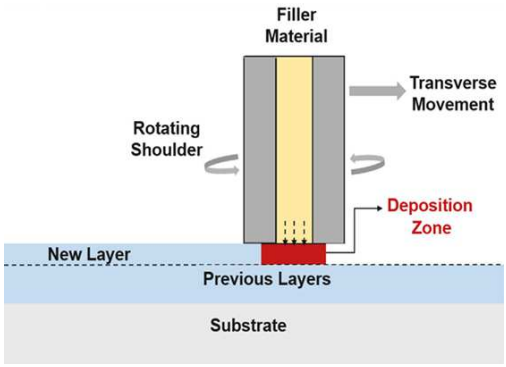

Figure 8: Principle of additive friction stir deposition [6]

Sample geometry

Similarly, single-cord and build-up samples were built using a MELD Manufacturing machine. Several AA7075 AFSD single-cord samples were investigated as shown in Fig. 9.a, with various sets of deposition parameters. For this process, only the AA7075 alloy was investigated. The substrate material is 6mm thick rolled AA7075, in T651 temper (peak-aged). The varying parameters are the traverse rate, the feeding rate, the temperature setpoint and the stepover amount (for multitracks only). Each layer is 2 to 3mm thick.

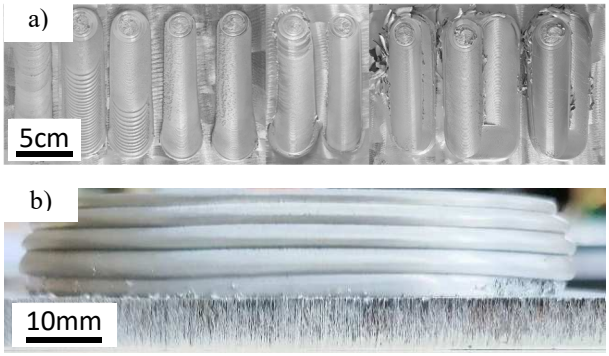

Figure 9: (a) AA7075 samples manufactured by AFSD: 3 of them are multitrack multilayer. (b) Lateral view of a multilayer sample.

Material health

Fig. 10 shows a cross-section of a single-cord sample. The material is fully dense and features a cohesive structure under the tool. Furthermore, the interface with the substrate is not sharp but diffuse on several hundred micrometers. This is a sign of steady mixing. Samples did not display porosity and crack, and no bending of the substrate was detected.
On the edge of the deposit material, the track exhibits flashings, which correspond to the zones where the feeding material has flowed without welding with the substrate. In application, they can be machined after deposition.

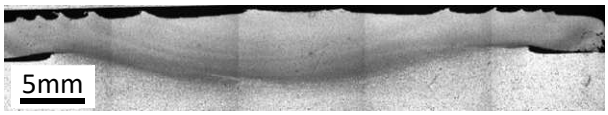

Figure 10: Optical picture of a cross-sectioned AFSD monolayer sample.

In what follows, if not specified otherwise, the multilayer sample associated with the best set of process parameters will be described, based on visual inspections and optical observation of cross-sections.

Microstructural characterization

Fig. 11 shows electron microscope images of three zones in the deposited material. In bulk material, grains are a few µm large and mostly equiaxed after recrystallization during deposition. No strong texture was detected. The microstructure also features both intra- and inter-granular precipitation. The biggest intermetallic compounds are either Mg and Si rich (the darkest ones) or Cu/Fe rich. Several families of smaller precipitates are present inside the grains and along grain boundaries. They are rich in Cu, Zn and Mg. The most notable family is the η phase ($MgZn_2$) which is the stable form of the η' nanometric phase. η' precipitates are known for being responsible of the hardening of aluminum 7xxx series: their density and size is of prime importance regarding mechanical properties [8].

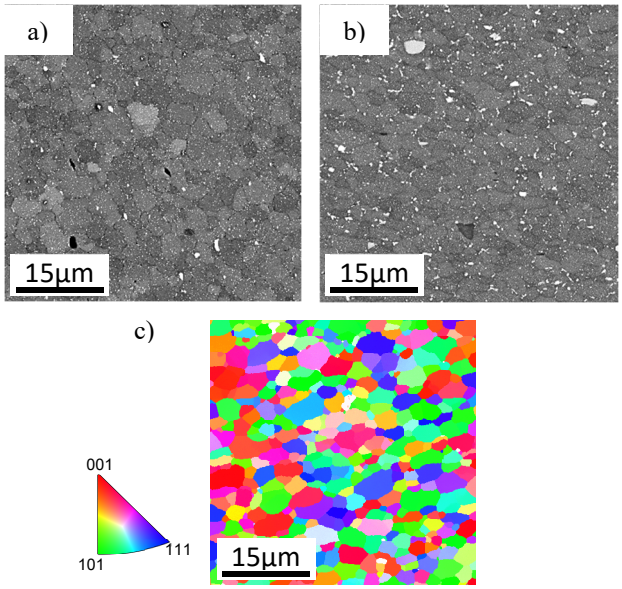

Figure 11: (a) SEM image of the last deposited layer. (b)-(c) SEM image and inverse pole figure of a bulk layer.

The microstructure is very similar in the last deposited layer, but precipitates are smaller and more dispersed. This is because the bulk layers (all but the last one) have undergone at least one additional heating cycle during the deposition of the following layers. At involved temperatures, smaller precipitates tend to coalesce in

bigger ones, leading to bulk's microstructure [9,10].

The interface's microstructure is displayed in Fig. 12: it is a mix between fully recrystallized grains from the feeding material and partially recrystallized in from the substrate. The latter are elongated and have iridescent colors in the inverse pole figure as they are still undergoing recrystallization.

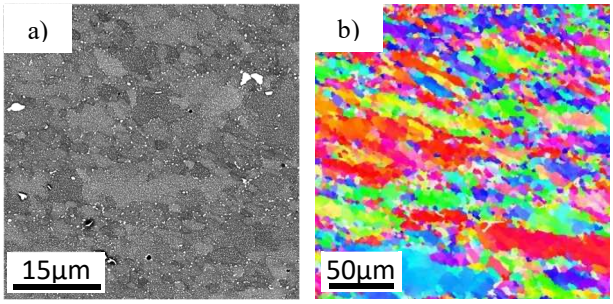

Figure 12: SEM image and inverse pole figure near the interface (the same color code as in Fig. 11 is used).

Finally, the substrate is depicted in Fig. 13. Compared to the metal before any deposition, the material in the heat-affected zone (HAZ) is characterized by precipitate growth, especially at grain boundaries, for the same thermal reasons explained before.

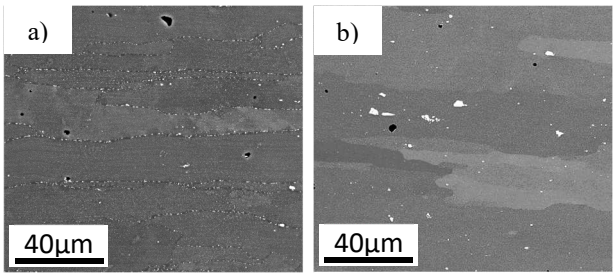

Figure 13: (a) SEM image of the HAZ. (b) SEM image of the substrate before deposition.

Mechanical response

In previous sections, heterogeneity and gradients have been described at the microstructural level. In what follows, they will be correlated with mechanical properties.

Fig. 14 displays a hardness map performed on the same monolayer sample as Fig. 10. Several observations can be noted:

- The deposition has greatly affected the substrate, as its hardness dropped from 180Hv to 100Hv in the HAZ. The hardness starts increasing again as the distance from the HAZ increases (e.g. on the sides).
- The deposited material has a good hardness (higher than 125Hv) but exhibits gradients (its local maximum is 155Hv).
- The smooth transition between deposited material and substrate suggests a good mixing.
- There is no local variation, which is consistent with the rather homogeneous microstructure at the considered scale (indents are 60µm large).

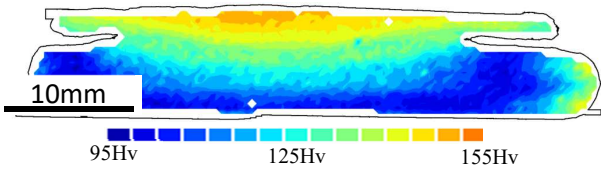

Figure 14: HV0.2 Vickers hardness map of a monolayer sample. Indents are separated by 300µm.

Regarding gradients, a hardness map of the multilayer sample is displayed Fig. 15. The maximum is achieved at the top of the build-up (last deposited layer), the hardness then decreases as the height decreases. Once again, no hardness jump was measured either at the interface or at the interlayers.

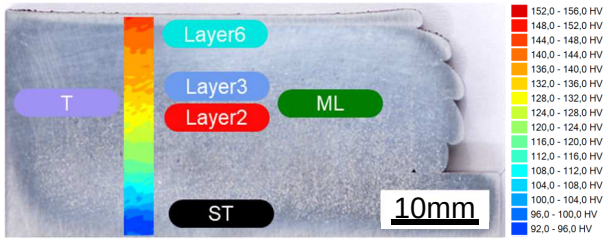

Figure 15: Vickers hardness maps of a multilayer sample. Seven indents were performed at every height.

Tensile behavior was also assessed Fig. 16. Classical strain rate of $10^{-3}s^{-1}$ was imposed on specimen sampled at various heights (see Fig. 15) and orientations, until failure. The yield stress and ultimate tensile stress vary accordingly with the hardness. The HAZ features the lowest yield stress of 170MPa, while the substrate's yield stress before deposition was 460MPa. In the bulk material, no major anisotropy was detected, and the elongation reached is 20% or higher. The last layer has the highest mechanical performances with $\sigma_{0,2}$=305MPa.

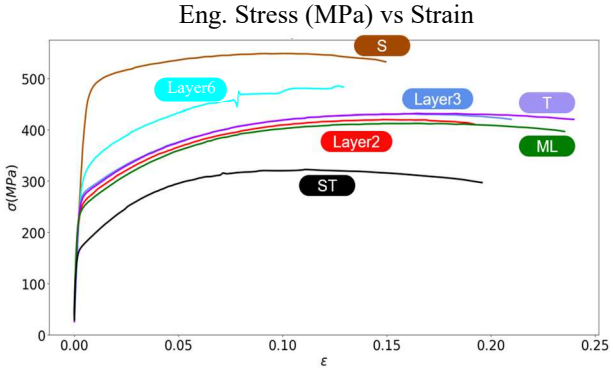

Figure 16: Engineering stress versus engineering strain for specimens at several locations of the build-up. T

stands for a transverse specimen, whereas others are in the longitudinal direction.

The fracture surfaces of theses specimens are reported Fig. 17. A change of failure mode is noted:

- In the substrate before deposition, cleavage is the dominant mode, with visible intergranular propagation.
- The deposited material is characterized by its ductile rupture mode: dimples cover the entire fracture surface. Microvoids also nucleate on intermetallic compounds.
- In the HAZ, both modes occur. The role of grain boundary precipitates growth is highlighted by dimples and voids surrounding these precipitates.

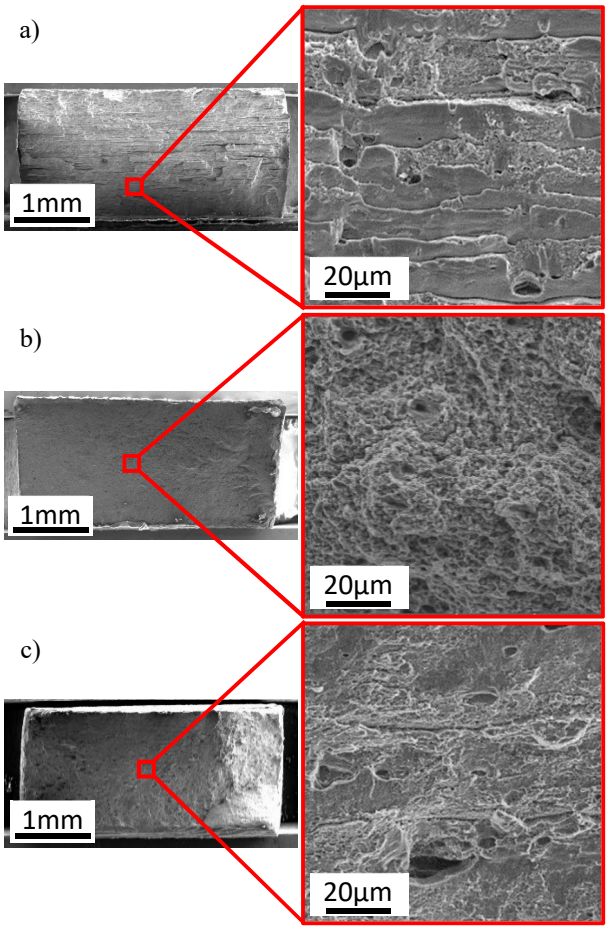

Figure 17: Fracture surfaces of tensile specimens. (a) Substrate before deposition. (b) Bulk material. (c) HAZ.

In order to understand the manifest link between microstructure and these diverse mechanical properties, *in situ* tensile test has been performed inside an electron microscope at LMS. Deformation was tracked using High Resolution Digital Image Correlation, based on a tin speckle pattern (see Fig. 18). Due to its size (smaller than the grain size), full-field local plastic deformation was computed using ONERA-developed Escale software [11], and displayed Fig. 19.

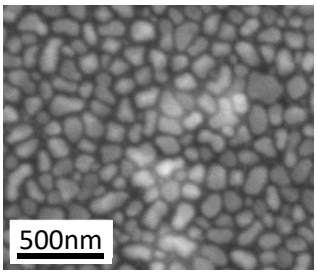

Figure 18: SEM image of the speckle pattern. The shape of a precipitate is visible by transparency.

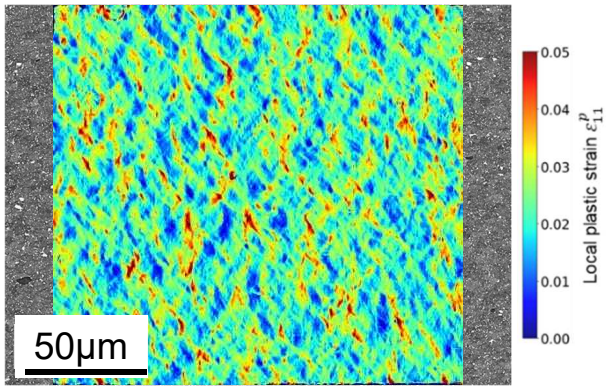

Figure 19: Plastic deformation map computed for a total deformation of 2.3% of a bulk deposited material specimen.

These tests are still under analysis. Preliminary results show deformation localization in the vicinity of certain features such as hard and brittle intermetallic compounds and specific grain boundaries, potentially leading to failure.

4. CONCLUSIONS & PERSPECTIVES

Optical microscopy and Scanning Electron Microscope analyses show that samples repaired by cold spray features a significant porosity level, even prohibitive, with delamination zones extending up to several centimeters long, depending on the parameters. These observations are confirmed by the hardness measurements, highlighting the abrupt transition between the substrate and the deposited material confirming poor adhesion.

On the contrary, the first characterizations of samples repaired by AFSD show a perfect material health and a smooth microstructure evolution through the repaired wall, confirmed by the hardness maps carried out on both monolayers and multitrack samples. Particular attention is paid to this microstructural evolution. Microstructure mapping by Electron BackScatter Diffraction gives access to the thermomechanical history of the repaired material. Microstructural characteristics such as grain size, crystallographic texture and local disorientation,

which are related to the level of deformation, provide an understanding of the microstructural changes during the remanufacturing step. In addition, first mechanical characterizations have been performed on specimens sampled at various heights of the repaired wall, allowing the assessment of the microstructural features on the mechanical response.

Finally, concerning the revalidation methodology, a more detailed characterization of the mechanical gradient was carried out, using Digital Image Correlation (DIC). These tests highlight the strain localization depending on the microstructure of the considered zone, i.e. initial substrate, HAZ or deposited material.

This first study on the feasibility of repair solutions using solid-state processes show very promising results obtained on the AFSD samples.

REFERENCES

1. Yin S., Cavaliere P., Aldwell B., Jenkins R., Liao H., Li W., Lupoi R. (2018). Cold spray additive manufacturing and repair: Fundamentals and applications, *Additive Manufacturing*, **21**, 628-650.
2. Stopyra W., Gruber K., Smolina I., Kurzynowski T., Kuźnicka B. (2020). Laser powder bed fusion of AA7075 alloy: Influence of process parameters on porosity and hot cracking, *Additive Manufacturing*, **35**, 101270.
3. Mauduit A., Pillot S., Gransac H. (2017). Study of the suitability of aluminum alloys for additive manufacturing by laser powder-bed fusion (2017), *Scientific Bulletin-University Politehnica of Bucharest*, **79**(4).
4. Rokni M.R, Widener C.A., Champagne V.K., Crawford G.A., Nutt (2017) S.R.. The effects of heat treatment on 7075 Al coldspray deposits, *Surface & Coatings Technology*, **310**, 278–285.
5. Rokni M.R., Widener C.A., Crawford G.A., West M.K. (2015). An investigation into microstructure and mechanical properties of cold sprayed 7075 Al deposition, *Material Science and Engineering: A*, **625**, 19–27.
6. A. Moridi, S. M. Hassani-Gangaraj, M. Guagliano & M. Dao (2014) Cold spray coating: review of material systems and future perspectives, Surface Engineering, 30:6, 369-395.
7. Yu H.Z., Jones M.E., Brady G.W., Griffiths R.J., Garcia D., Rauch H.A., Cox C.D. & Hardwick N. (2018). Non-beam-based metal additive manufacturing enabled by additive friction stir deposition, *Scripta Materialia*, **153**, 122-130.
8. Fuller C.B., Mahoney M.W., Calabrese M. & Micona L. (2010). Evolution of microstructure and mechanical properties in naturally aged 7050 and 7075 Al friction stir welds, *Materials Science and Engineering: A*, **527**(9), 2233-2240.
9. Milkereit B., Österreich M., Schuster P., Kirov G., Mukeli E., & Kessler O. (2018.) Dissolution and Precipitation Behavior for Hot Forming of 7021 and 7075 Aluminum Alloys, *Metals*, **8**(7), 53.
10. Garcia D., Hartley W.D., Rauch H.A., Griffiths R.J., Wang R., Kong Z.J., Zhu Y. & H.Z. Yu (2020). In situ investigation into temperature evolution and heat generation during additive friction stir deposition: A comparative study of Cu and Al-Mg-Si, *Additive Manufacturing*, **34**, 101386.
11. Feld-Payet S., Fourest T., Bouda P., Garaud J.D., Bettonte F., Tireira A., Le Sant Y., Le Besnerais G. & Belon S. (2022). Escale: une plateforme ouverte pour le dialogue essai-modèle-calcul In *Proceedings 15ème du Colloque National en Calcul des Structures CSMA*, Giens.